Effects of induction and wake steering control on power and drivetrain responses for 10 MW floating wind turbines in a wind farm

Effects of induction and wake steering control on power and drivetrain responses for 10 MW floating wind turbines in a wind farm

Dirk Willem van Binsbergen, Shuaishuai Wang, Amir R. Nejad

Department of Marine Technology, Norwegian University of Science and Technology (NTNU), Otto Nielsens veg 10, 7052 Trondheim, Norway

E-mail: diederiv@stud.ntnu.no

Abstract. This paper aims to investigate the drivetrain load response caused by induction and wake steering control on two floating wind turbines (FWTs) in a wind farm. In this study, two DTU 10 MW turbines, supported on the nautilus floater, are modelled using FAST.Farm. The downstream turbine is placed at the distance of seven rotor diameters (D) from the upstream turbine in the positive wind direction. Partial wake shading is considered for wake steering control and full wake shading is considered for induction control. An ambient wind speed of 8m/s is used and a representative sea state is selected. The test cases are defined based on different blade pitch and yaw angles of the upstream turbine. Power generation of the offshore wind farm is studied under different test cases. A decouped analysis approach is used to investigate drivetrain response. Global responses are obtained from FAST.Farm. These loads are used as input of the 10 MW wind turbine drivetrain model for the gears and bearings load response analysis. Results show that both induction and wake steering control lead to a limited increase in power generation of the wind farm. Additionally, both control methods affect the drivetrain response statistics, while the features are different. This study facilitates a better understanding on drivetrain dynamic behaviour in a wind farm perspective, which serves as a reference for the wind farm optimizaton in the future.

1. Introduction

Wind farm control has received significant attention in recent years. Wind turbine wakes, characterized by a velocity deficit and added turbulence, could significantly affect the total power production and fatigue life of turbines within a farm. More specifically, the velocity deficit behind the upstream turbine results in a power loss of downstream turbines, whereas the added turbulence causes the increase in structural loads of downstream turbines leading to the increase in fatigue damage [1].

Many studies have been conducted to investigate the dynamic behaviour of wakes or wake effects on wind turbines [1]-[3] and some studies have been carried out on the wind farm control [4]-[12], while studies on the load effect analysis of the drivetrains in wind farms have not yet been conducted. It is known that the drivetrain is the most vulnerable part in the wind turbine system and its downtime would pose huge loss of the cost of the wind turbine [13]-[15]. Hence, reducing the drivetrain loads and improving its working life should be taken into account when performing wind farm optimization.

The objective of this study is to get more insight into the power performance and drivetrain dynamic behaviour of floating wind turbines in a wind farm. To achieve this objective, an offshore wind farm which consists of two 10 MW floating turbines is established using OpenFAST and FAST.Farm [16]-[20]. Moreover, effects of yaw and blade pitch control on power generation and drivetrain dynamic response of the two 10 MW floating turbines are studied.

2. Methodolgy

2.1. FAST.Farm model

FAST.Farm is a midfidelity multiphysics engineering tool able to predict the power performance and structural loads of wind turbines within a wind farm which has been developed by the National Renewable Energy Laboratory (NREL). FAST.Farm is based on the Dynamic Wake Meandering (DWM) model and uses instances of OpenFAST to compute the aero-hydro-servo-elastic dynamics of each turbine separately.

2.1.1. Wind Field Setup The wind field size is chosen to be X × Y × Z = 10 km × 952.5 m × 472.5 m, which is referred by the study of Wise et al. [21]. The low-resolution domain ΔX, ΔY and ΔZ is found to be 1.376 m, 7.5 m and 7.5 m with a timestep of 2 s [19]. The high-resolution domain has an identical spacial resolution, but a different timestep of 0.125 s [22].

The high resolution wind field is located around the FWT, whereas the low resolution wind field covers the rest of the wind field. The number of high resolution nodes NX_{high}, NY_{high} and NZ_{high} are taken to be 102, 64 and 32 nodes, which results in a high resolution wind field of the dimensions of $X_{high} \times Y_{high} \times Z_{high}$ = 139m × 472m × 232.5m where the high resolution wind field starts 80m in upwind direction from each individual turbine.

The wind field is created using the Mann turbulence model [23], which can be generated using a pre-processor tool of HAWC2 [24]. The Mann turbulence model is a three dimensional velocity spectral tensor and is defined in IEC61400-1 [25]. The model depends on 3 variables: $\alpha\epsilon^{2/3}$, L and Γ. $\alpha\epsilon^{2/3}$ is the energy dissipation rate parameter, L is the length scale describing the eddy size that mainly contains the energy and Γ is the shear distortion parameter. ϵ is the rate of viscous dissipation of turbulent kinetic energy and α is the three-dimensional Kolmogorov constant equal to 1.7 [26]. $\alpha\epsilon^{2/3}$, L and Γ are found to be $0.144\text{m}^{4/3}\text{s}^{-2}$, 33.6m and 3.9, respectively. The simulation time is 4000s, with a 400s transient and an output timestep of 0.025s.

2.1.2. Arrangement Two turbines are placed in the wind field with the hub coordinates described in Table 1 and the yaw control layout shown in Figure 1, where FWT_1 is the upstream turbine and FWT_2 is the downwind turbine. The layout is based on Gebraad (2014) [27] and Kanev (2020) [8] with an absolute distance of 7 rotor diameters, D.

Table 1. Turbine hub coordinates above SWL in the generated wind field (Left: yaw control; right: blade pitch control).

Turbine number [-]	X [km]	Y [m]	Z [m]	X[km]	Y [m]	Z [m]
1	1	-89.15	119	1	0	119
2	2.245	0	119	2.248	0	119

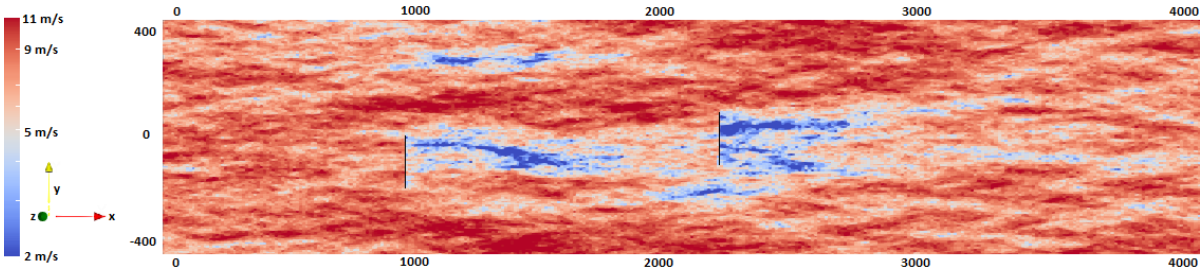

Figure 1. Turbulent Wind Field of the reference yaw case (TC_0) where the wind flows in positive X direction.

2.2. OpenFAST model

The WT model used in OpenFAST is the DTU 10 MW reference wind turbine [28], which is supported by the nautilus semi-submersible floater [16, 28]. This floater is developed in the LIFES50+ project, which aims to develop new innovative substructure concepts. The floater is symmetric and consists of four columns, which connect the main frame by an X-shaped deck and a square-shaped ring pontoon on the top and the bottom, respectively. The model used can be seen in Figure 2.

The mooring lines are modelled using MoorDyn [29] for a water depth of 130m and an unstretched length of 833.24m. On one side, they connect the columns, and on the another side, they are fixed to the seabed by drag anchors for station keeping.

The tower is modelled with a traditional approach where the tower is flexible from the nacelle to the floating substructure.

The rotor diameter is D = 178.3m and the hub height is z_{hub} = 119m above still water level (SWL). These values have not been changed from the original DTU 10 MW reference turbine. The rotor aerodynamics have been updated to AeroDyn v15 [30].

The DTU wind energy controller of the DTU 10 MW reference WT was tuned to avoid resonance of the nautilus 10 MW WT, which is explained in Larsen et al. [31]. The blade pitch angle (B.P. angle) and yaw angle have been modified in the ServoDyn module to create the desired test cases and constant power control is used above rated for maximum power production.

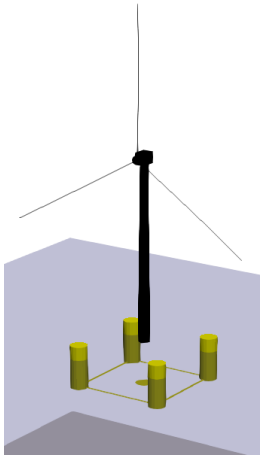

Figure 2. Computational model of the nautilus 10 MW WT visualized in OpenFAST with lines representing the prebent blades. The tower and nacelle are colored black while the hydrodynamic members are colored yellow [21].

2.3. Drivetrain model

In this paper the 10 MW reference drivetrain developed by Wang et al. [32] was used. The drivetrain adopts a four-point support configuration and a medium-speed gearbox which consists of two planetary stages and one parallel stage, with a total transmission ratio of 1:50. The drivetrain topology with gear and bearing nomenclatures is shown in Figure 3. The drivetrain dynamic model is established using a multi-body system (MBS) simulation tool SIMPACK [34], which is presented in the Figure 4.

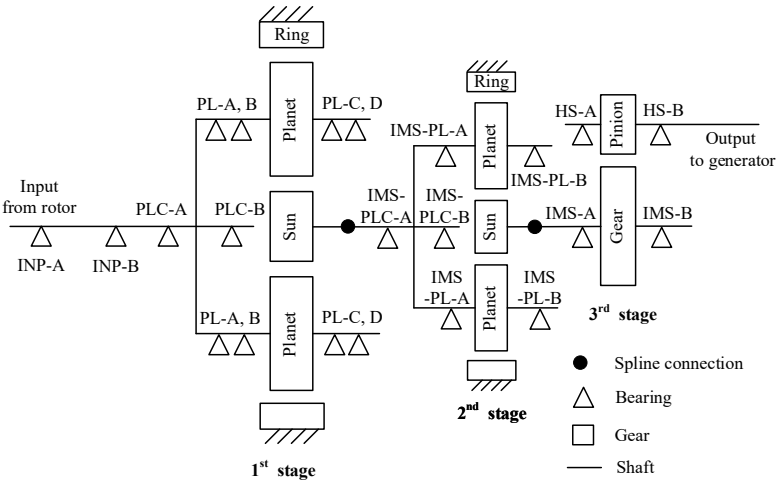

Figure 3. 10MW reference drivetrain topology [32]

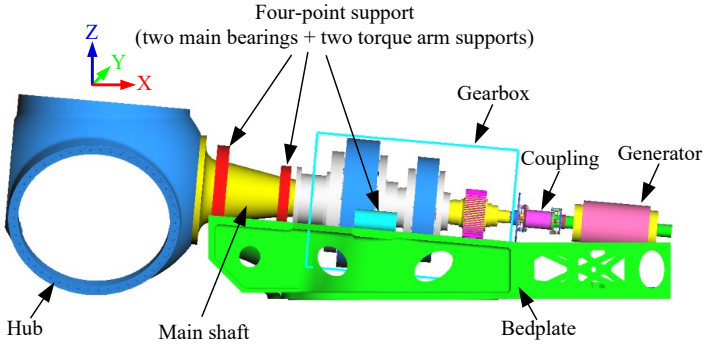

Figure 4. 10MW drivetrain numerical model [32]

2.4. Decoupled analysis method

A decoupled analysis method is used to calculate the drivetrain dynamic load responses in this study. First, Global forces and moments of the two FWTs are obtained using the program FAST.Farm. Then, these time series of forces and moments are applied at the hub center of the drivetrain models to calculate gear and bearing load effects.

2.5. Environmental conditions and test cases

The environmental conditions are based on a deep water site in the North Sea. A mean wind speed at hub height, u_{hub}, of 8 m/s is chosen. Wind turbine class B is selected in this study, and

the power law exponent, α, is taken as 0.14. The value of the turbulence standard deviation in the positive wind direction, σ_u, is determined as follows:

$$\sigma_u = I_{ref}\,(0.75u_{hub} + b)\,; b = 5.6m/s \tag{1}$$

The significant wave height, H_s, is determined using Beaufort scale linear interpolation, whereas the corresponding peak period, T_p, is found using IEC61400-3 [33], where H_s = 2.0m and T_p = 7.4s. The current is not taken into account in this paper.

A total of 10 test cases are described in Table 2. The test cases are determined through iteration in FAST.Farm for optimal power generation. The B.P. angle and yaw angle are both modified respectively in the ServoDyn module. Test case 0 is the baseline test case for wake steering control and test case 5 is the baseline test case for axial induction control. Test case 1 to 4 are test cases where the yaw angle is modified to steer the wake. Test case 6 to 9 are test cases where the B.P. angle is modified to change the axial induction factor of the upwind wind turbine. In this study, all the test cases are applied on the first turbine, by which investigating the effects of yaw and B.P. controls on power generation and drivetrain load effects of both turbines.

Table 2. Considered test cases of turbine 1 for this work.

	Test case number [-]	Blade pitch angle [-]	Yaw angle [°]
Reference	TC_0	0	0
Yaw control	TC_1	0	5
	TC_2	0	7
	TC_3	0	8
	TC_4	0	10
Reference	TC_5	0	0
Pitch control	TC_6	1	0
	TC_7	2	0
	TC_8	3	0
	TC_9	4	0

3. Results and discussions

3.1. Effects on power generation

The power production, thrust, torque and bending moment of each test case are compared between the two turbines. The comparisons of power production and response statistics of drivetrain input loads are demonstrated in the Figure 5 and Figure 6, respectively. Also, Table 3 shows the total power production increase of TC_1-TC_4 where TC_0 is taken as the baseline case and of TC_6-TC_9 where TC_5 is taken as the baseline case.

Table 3. Power production change normalised to TC_0 for TC_1-TC_4 and normalised to TC_5 for TC_6-TC_9.

Test case	TC_1	TC_2	TC_3	TC_4	TC_6	TC_7	TC_8	TC_9
Power production change [%]	0.70	0.78	0.73	0.60	0.17	0.02	-0.86	-2.24

From Figure 5 and Table 3, it is observed that the total power of the two FWTs shows a limited increase and then decreases over both the yaw angle and the B.P. angle, where the power production of turbine 1 is decreasing while the power production of turbine 2 is increasing. The

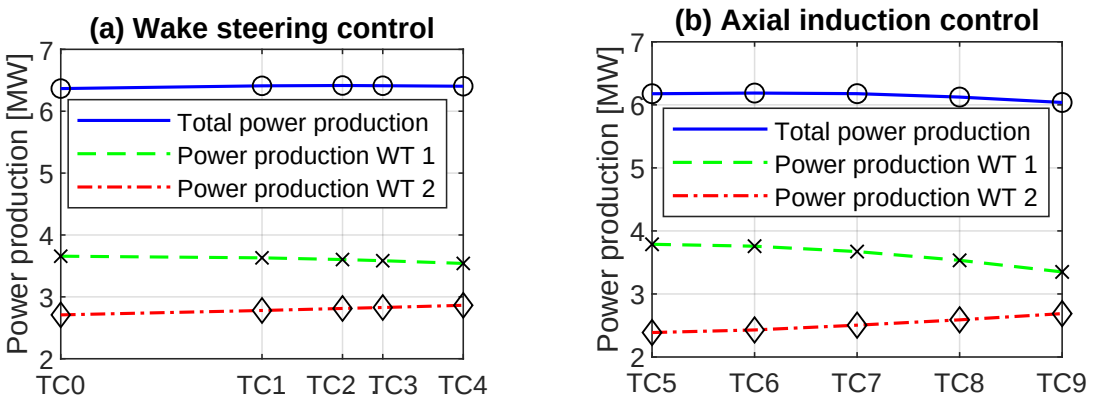

Figure 5. Total power production and power production of FWT_1 and FWT_2 for each test case.

limited increase in power production can be explained by the high turbulence intensity of 0.203, causing faster wake mixing behind the upwind turbine wake.

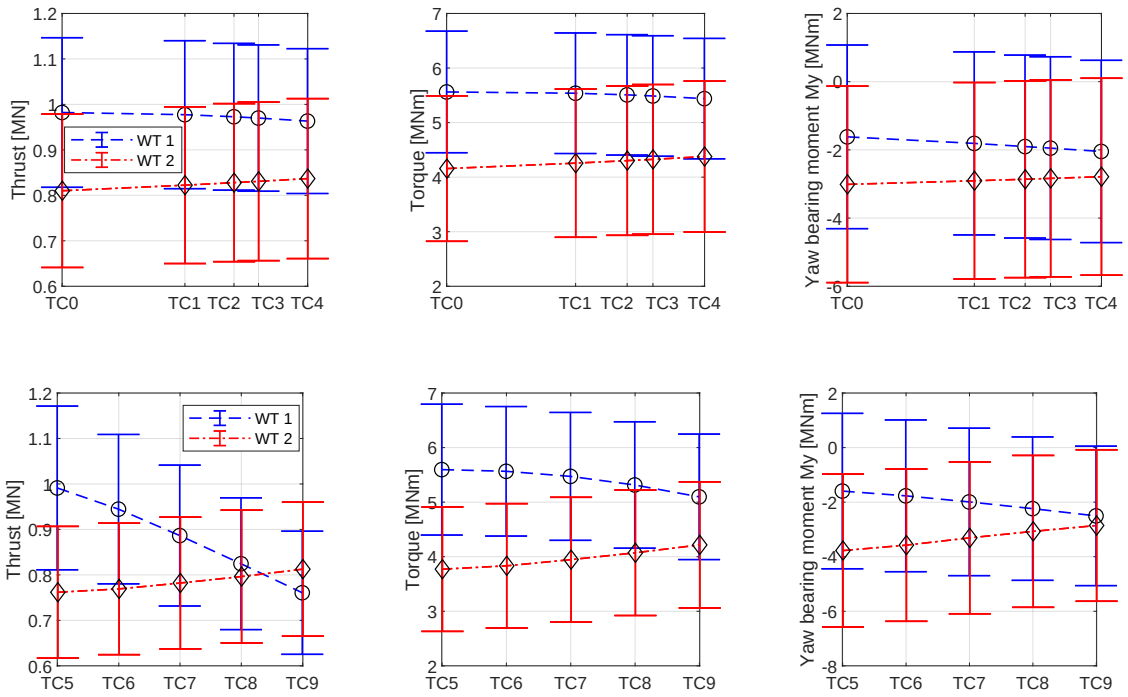

Figure 6. Mean values and standard deviations of the thrust (Fx), torque (Mx) and bending moment (My) at the yaw bearing for each test case (First line: yaw control; second line: blade pitch control).

Figure 6 presents the mean values and standard deviations of global thrust force Fx, torque Mx and the yaw bearing bending moment My of the two turbines under all test cases. The bending moment My acts on the tower top and is of opposite value when used for the drivetrain model. The coordinates used in this figure are shown in Figure 4. In the yaw control scenario,

it is found the feature of mean values of Fx and Mx of the two turbines is approximately consistent with that of the power production; namely, they decrease for FWT_1 and increase for FWT_2 as the yaw angle increases. In contrast, the mean values of bending moment My at the yaw bearing for FWT_2 are higher than for FWT_1 under all test cases and they increase for FWT_1 and decrease for FWT_2 as the yaw angle increases. The moment is negative due to the weight of the hub and blades creating a larger moment than Fx. An increase in Fx will decrease the magnitude of My. Note that this is not the overturning moment at the tower base.

In the pitch control scenario, the feature of torque Mx of the two turbines are consistent with that of the power production; namely, the values of turbine 1 decrease and turbine 2 increase slightly as the pitch angle increases. In contrast, the mean values of bending moment My for FWT_2 are higher than for FWT_1 under all test cases and they increase for FWT_1 and decrease for FWT_2 as the pitch angle increases. The mean value of the thrust force of FWT_1 is different with that of the power and torque values. The mean value decreases rapidly passing the mean thrust value of FWT_2 between TC_8 and TC_9. Both FWT_1 and FWT_2 vary linearly with the increase of pitch angle. Pitching the WT blades will result in a decreased value for the axial induction factor, which explains the behavior of Fx.

Table 4. Change of the mean values and standard deviations for yaw control cases with test case 0 as baseline. Green indicates the mean of a bearing or gear that decreased with more than 5% for TC_4, red indicates the mean of a bearing or gear that increased with more than 5% for TC_4 and orange indicates the remaining bearings and gears.

Gear, bearing load	FWT_1							
	mean value				standard deviation			
	TC_1	TC_2	TC_3	TC_4	TC_1	TC_2	TC_3	TC_4
INP-A, axial	-1	-1	-2	-2	-1	-2	-2	-2
INP-A, radial	3	4	5	6	1	2	2	3
INP-B, axial	-1	-2	-2	-3	-1	-2	-2	-2
INP-B, radial	-1	-2	-3	-3	-1	-1	-1	-2
HS-B, radial	-1	-2	-5	-9	-1	-1	-1	-2
1st, sun-planet	-1	-1	-2	-3	-1	-2	-2	-2
2nd, sun-planet 3rd, gear-pinion					-2	-2	-2	-2
Gear, bearing load	FWT_2							
	mean value				standard deviation			
	TC_1	TC_2	TC_3	TC_4	TC_1	TC_2	TC_3	TC_4
INP-A, axial	2	3	3	4	1	2	2	2
INP-A, radial	-1	-1	-1	-2	0	0	0	0
INP-B, axial	3	4	5	6	2	2	2	3
INP-B, radial	0	0	1	1	1	1	1	1
HS-B, radial	2	3	4	5	2	3	3	4
1st, sun-planet					3	3	5	5
2nd, sun-planet 3rd, gear-pinion					2	3	4	4

3.2. Effects on drivetrain dynamic response

Table 4 and Table 5 list the percentual change of drivetrain response statistics for cases with and without yaw control and pitch control, respectively. Relative values of each test case are presented in these tables. Representative gears and bearings, INP-A, INP-B, HS-B and three stage gear pairs, are selected to analyze in this study. The layout of these gears and bearings is illustrated in Figure 3. Figure 7 and Figure 8 show the INP-A and INP-B radial and axial loads, as well as the the gear-pinion loads. In general, effects on drivetrain dynamic response

Table 5. Change of the mean values and standard deviations for pitch control cases with test case 5 as baseline. Green indicates the mean of a bearing or gear that decreased with more than 5% for TC_7, red indicates the mean of a bearing or gear that increased with more than 5% for TC_7 and orange indicates the remaining bearings and gears.

Gear, bearing load	FWT$_1$							
	mean value				standard deviation			
	TC_6	TC_7	TC_8	TC_9	TC_6	TC_7	TC_8	TC_9
INP-A, axial	-6	-14	-22	-31	-7	-11	-15	-18
INP-A, radial	-1	-2	-3	-4	-2	-4	-6	-8
INP-B, axial	-8	-18	-28	-38	-7	-11	-15	-20
INP-B, radial	-1	-3	-5	-6	-1	-4	-6	-8
HS-B, radial	-1	-2	-5	-9	-1	-3	-4	-5
1st, sun-planet	-1	-2	-5	-9	-1	-8	-2	-3
2nd, sun-planet					-1	-2	-3	-4
3rd, gear-pinion								
Gear, bearing load	FWT$_2$							
	mean value				standard deviation			
	TC$_6$	TC$_7$	TC$_8$	TC$_9$	TC$_6$	TC$_7$	TC$_8$	TC$_9$
INP-A, axial	1	4	7	10	0	0	1	1
INP-A, radial	-3	-6	-8	-10	-1	-2	-2	-3
INP-B, axial	2	6	10	14	0	0	2	2
INP-B, radial	1	2	3	4	0	0	1	2
HS-B, radial	2	5	8	12	0	1	1	2
1st, sun-planet					0	0	0	2
2nd, sun-planet					0	0	0	0
3rd, gear-pinion								

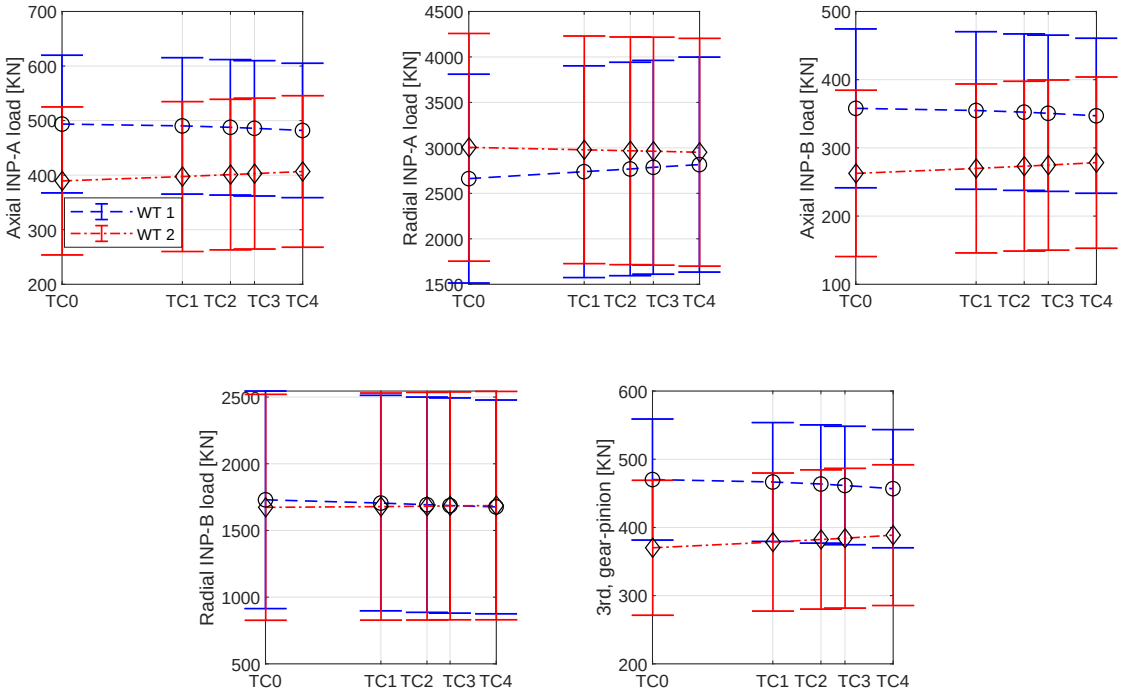

Figure 7. Mean values and standard deviations of the axial and radial INP-A and INP-B bearing loads and the 3rd gear-pinion load for each yaw test case.

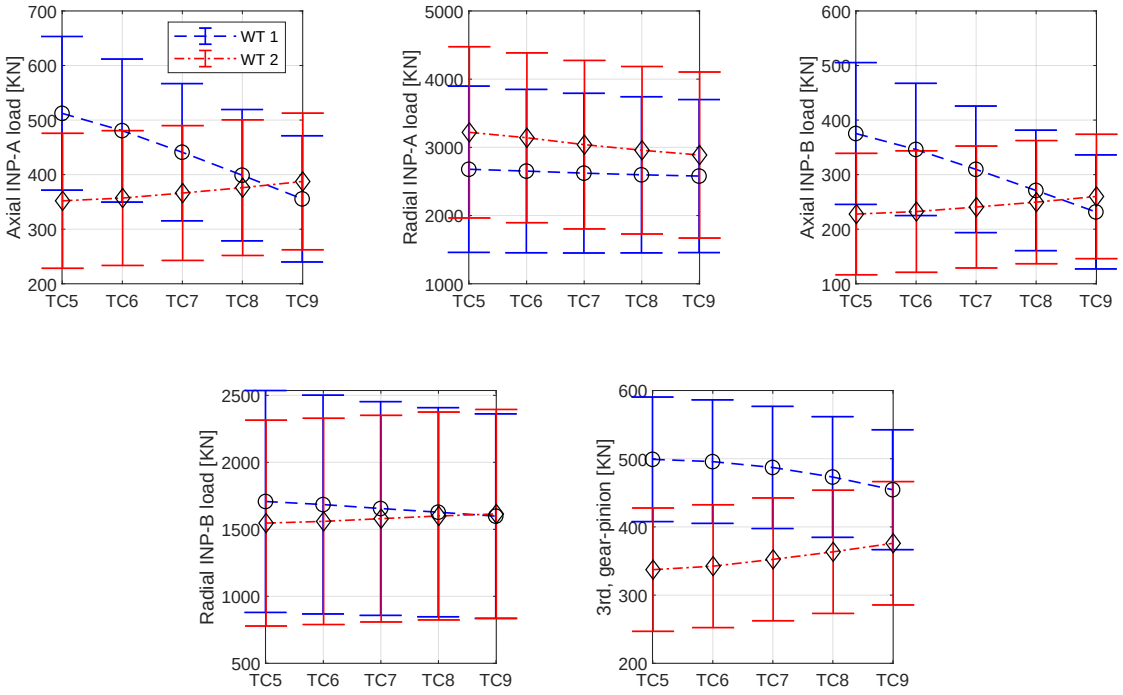

Figure 8. Mean values and standard deviations of the axial and radial INP-A and INP-B bearing loads and the 3rd gear-pinion load for each blade pitch test case.

induced by pitch control are larger than by yaw control, because pitch control results in larger global load variations than the yaw control under test cases defined in this study. Effects on mean values of drivetrain loads of the two wind turbines are observed with same features in the two control scenarios. More specifically, the feature of mean values of axial forces of INP-A and INP-B is close with that of the global thrust force shown in Figure 6, because main bearing axial forces are mainly induced by global thrust loads. Additionally, feature of mean load response of gears and bearings inside the gearbox, HS-B radial load and three stage gear tooth contact loads, is observed to be close with that of the global torque loads with the increase of the test cases, which is because the gearbox load response is mainly dominated by torque loads. The radial loads of main bearings are mainly induced by rotor blade and main shaft weight as well as vertical force and bending moments produced by the rotor, thus the feature of mean values of INP-A radial force is corresponding with the yaw bearing bending moment My shown in Figure 6. It is noted that the radial stiffness of upwind main bearing INP-A is larger than the downwind bearing INP-B, which lead to the majority of radial loads are carried by the INP-A and this accounts for the fact that both the yaw control and pitch control have very small effects on mean values of INP-B radial loads. In addition, both the yaw control and pitch control affect standard deviations of drivetrain load response of the two turbines, while characteristics of the effects induced by these two control scenarios differ. It is observed that pitch control generally induces larger effects on the drivetrain standard deviation response of FWT_1 than FWT_2, while it is opposite with the effects induced by the yaw control. Reason for this is revealed by load spectra analysis. Figure 9 and Figure 10 compare the axial force spectra of main bearing INP-A in the two turbines between TC_0 and TC_4 as well as TC_5 and TC_9, respectively. It is found that all the load spectra are dominated by the wave frequency response as well as the rotor 3P and

6P response. Peak values at the wave frequency are very close in all of the load spectra, while those at the rotor 3P and 6P frequencies differ in the spectra of Figure 9 and Figure 10. The 3P and 6P response for TC_4 and TC_0 are very close. A small decrease in 3P and 6P response is found for FWT_1 and a small increase is found for FWT_2. For TC_5 and TC_9 a frequency shift is found for the 3P and 6P response due to the decrease in angular velocity of the main shaft, where the peaks do not change significantly. For FWT_2 a small decrease in 3P and 6P response is found.

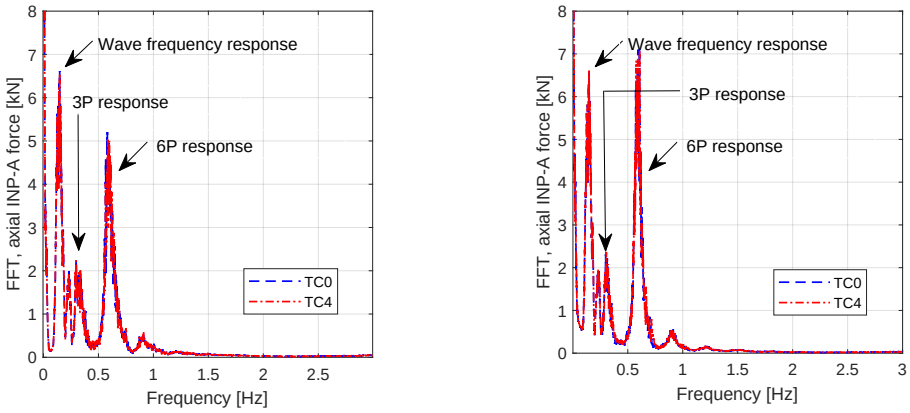

(a) WT_1 (b) WT_2

Figure 9. Comparison of the axial force spectra of main bearing INP-A between TC_0 and TC_4.

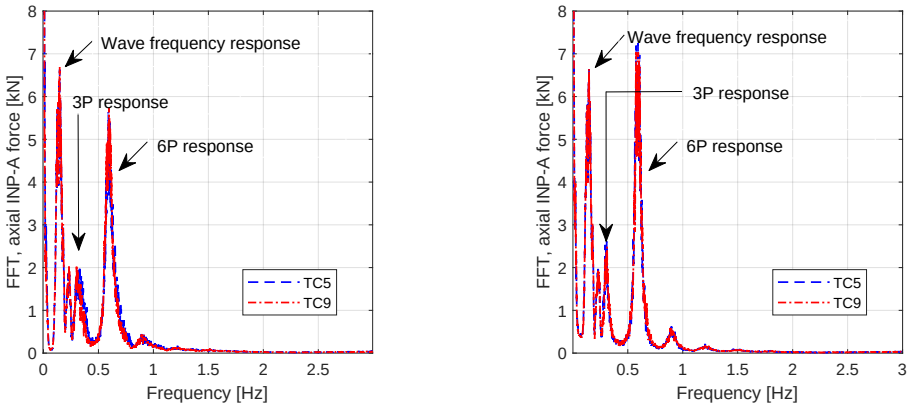

(a) WT_1 (b) WT_2

Figure 10. Comparison of the axial force spectra of main bearing INP-A between TC_5 and TC_9.

4. Concluding remarks

This study deals with the effects of induction and wake steering controls on power generation and drivetrain load response in an 10 MW offshore wind farm perspective. The wind farm consists of two 10 MW floating wind turbines supported on the nautilus floater. The wind farm models are developed using FAST.Farm and the 10 MW floating wind turbines are built using the software OpenFAST. In addition, a high-fidelity drivetrain model, which is established using

multi-body system method, is employed. Environmental conditions which consist of turbulent wind and irregular waves are presented. Induction control and wake steering control are realized via defining the blade pitch and yaw angles on the upwind turbine. Effects of these two control scenarios on the wind farm power generation and drivetrain dynamic response are investigated.

The upstream turbine power is decreasing while the downstream turbine power is increasing for as the pitch and yaw angles increase. Global torque and thrust loads of individual turbines vary with approximately identical feature of their power production as the yaw angles increase. Global torque loads of individual turbines vary with approximately identical features of their power production as the blade pitch angle increases, while the upstream turbine thrust load decreases significantly as the blade pitch angle increases. Effects of the induction and wake steering control on mean values of drivetrain load effects are generally identical with that of the global load response. Wake steering control does not have large effects on drivetrain standard deviation response of the upstream turbine, while the increase of yaw angle would lead to the increase of drivetrain standard deviation response of the downstream turbine, which is due to partial shading of the downstream turbine. As a contrast, the increase of blade pitch angle would lower the standard deviations of drivetrain dynamic response of the upstream wind turbine, while it does not affect the standard deviations in the downstream turbine significantly. This is due to the 3P and 6P response of drivetrain gears and bearings being different in the two turbines under the two control strategies.

Acknowledgments

Thank you to Jason Jonkman from NREL for providing us with the FAST.Farm software and thank you to Erin Bachynski and Adam Wise from NTNU and UC Berkeley for assistance regarding the model and FAST.Farm software.

References

[1] Öztürk E. Wake induced power deficit analysis on wind turbines in forested moderately complex terrain using SCADA data [dissertation on the Internet]. University of Uppsala; 2018. URL `http://urn.kb.se/resolve?urn=urn:nbn:se:uu:diva-346639`

[2] Kirby A, Hassanzadeh A, Mavriplis D J and Naughton D 2018 *36th Wind Energy Symposium* (Kissimmee, Florida: American Institute for Aeronautics and Astronautics) ISBN: 978-1-62410-522-7, URL `https://arc.aiaa.org/doi/pdf/10.2514/6.2018-0256`

[3] González-Longatt F, Wall P. and Terzija V 2012 *Renewable Energy* **39** 329-38 ISSN 0960-1481, URL `https://doi.org/10.1016/j.renene.2011.08.053`

[4] Bossanyi E 2018 *J. Phys.: Conf. Series* **1037** 032011

[5] Siniscalchi-Minna S, Bianchi F D, De-Prada-Gil M and Ocampo-Martinez C 2019 *Renewable Energy* **131** 37-44 ISSN 0960-1481, URL `https://doi.org/10.1016/j.renene.2018.06.112`

[6] Howland M, Lele S K and Dabiri J O 2019 *Wind farm power optimization through wake steering* Proceedings of the National Academy of Sciences **116** 14495-14500 URL: `https://www.pnas.org/content/116/29/14495.short`

[7] Mirzaei M, Göçmen T, Giebel G, Sørensen P E and Poulsen N K 2015 *American Control Conference* (Illinois: Chicago) 1709-14 URL: `https://ieeexplore.ieee.org/document/7170979`

[8] Stoyan Kanev 2020 Dynamic wake steering and its impact on wind farm power production and yaw actuator duty *Renewable Energy.* **146** 9-15 ISSN 0960-1481 URL `https://doi.org/10.1016/j.renene.2019.06.122`

[9] van Dijk M T, van Wingerden J W, Ashuri T and Li Y 2017 *Energy* **121** 561-9

[10] Gebraad P, Teeuwisse F, van Wingerden J W, Fleming P, Ruben S, Marden J and Pao L 2014 *Wind Energy* **19** 95-114

[11] Fleming P A, Gebraad P M, Lee S, van Wingerden J W, Johnson K, Churchfield M, Michalakes J, Spalart P and Moriarty P 2014 *Renewable Energy* **70** 211-8

[12] Kanev S 2019 *Renewable Energy* **146** 9-15

[13] Sheng S S 2013 *Report on Wind Turbine Subsystem Reliability A Survey of Various Databases* National Renewable Energy Laboratory (NREL)

[14] Njiri J G, Beganovic N, Do M H and Söffker D 2019 *Renewable Energy* **131** 818-28 ISSN 0960-1481, URL: https://doi.org/10.1016/j.renene.2018.07.109
[15] Spinato F, Tavner P J, Bussel J W V and Koutoulakos E 2009 *IET Renewable Power Generation* **3** 387-401,
[16] Pegalajar-Jurado A et al. 2018 *State-of-the-art models for the two LIFES50+ 10 MW floater concepts* Tech. Rep. D4.5, LIFES50+
[17] Jonkman J M 2019 *OpenFAST Documentation, release v2.1.0* Tech. Rep. National Renewable Energy Laboratory
[18] Jonkman J M Marshall L Buhl Jr 2005 *FAST User's Guide* Tech. Rep. NREL/EL-500-38230, National Renewable Energy Laboratory
[19] Jonkman J M *FAST.Farm User's Guide and Theory Manual* Tech. Rep. NREL/TP-xxxx-xxxxx, National Renewable Energy Laboratory
[20] Jonkman J M, Annoni J, Hayman G, Jonkman B, Purkayastha A 2017 *Development of FAST.Farm: A New Multi-Physics Engineering Tool for Wind-Farm Design and Analysis* (Kissimmee, Florida: American Institute of Aeronautics and Astronautics)
[21] Wise A S, Bachynski E E. Wake meandering effects on floating wind turbines *Wind Energy.* 2020; 1– 20, URL: https://doi.org/10.1002/we.2485
[22] Shaler K, Jonkman J and Hamilton N 2019 Effects of inflow spatiotemporal discretization on wake meandering and turbine structural response using FAST.Farm. *J. Phys.: Conf Series* **1256** (012023) URL: https://doi.org/10.1088/1742-6596/1256/1/012023
[23] Mann J 1994 The spatial structure of neutral atmospheric surface-layer turbulence *Journal of fluid mechanics* **273** 141-168
[24] DTU Wind Energy. Pre-processing tools - HAWC2.2014. URL: http://www.hawc2.dk/download/pre-processing-tools
[25] International Electrotechnical Commision (IEC) 2005 *Wind turbines- Part 1: Deign Requirements* Tech. Rep. IEC61400-1
[26] Cheynet E, Jakobsen J B, and Obhrai C. 2017 Spectral characteristics of surface-layer turbulence in the north sea. *Energy Procedia*, **137** 414 – 427
[27] P.M.O. Gebraad. *Data-Driven Wind Plant Control.* PhD thesis, TU Delft, 2014.
[28] DTU 10 MW Reference Wind Turbine URL: https://rwt.windenergy.dtu.dk/dtu10MW/dtu-10MW-rwt
[29] Hall M 2017 *MoorDyn User's Guide* Techn. Rep. , Department of Mechanical Engineering, University of Maine
[30] Jonkman J M, Hayman G J, Jonkman B J and Damiani R R *AeroDyn v15 User's Guide and Theory Manual* Techn. Rep. NREL/TP-xxxx-xxxxx, National Renewable Energy Laboratory
[31] Larsen T and Hanson T 2007 A method to avoid negative damped low frequent tower vibrations for a floating, pitch controlled wind turbine. *J Phys.: Conf Series* **75** 012073
[32] Wang S, Nejad A R and Moan T. On design, modelling, and analysis of a 10-MW medium-speed drivetrain for offshore wind turbines *Wind Energy.* 2020; 1– 19, URL: https://doi.org/10.1002/we.2476
[33] International Electrotechnical Commision (IEC) 2009 *Wind turbines- Part 3: Deign Requirements for offshore wind turbines* Tech. Rep. IEC61400-3
[34] Dassault Systemes - SIMPACK. URL: https://www.3ds.com/products-services/simulia/products/simpack/